Sensors & Diagnostics

COMMUNICATION



Cite this: *Sens. Diagn.*, 2023, **2**, 262

Received 8th October 2022,
Accepted 28th December 2022

DOI: 10.1039/d2sd00177b

rsc.li/sensors

# Discriminative 'turn-on' fluorescence sensing of volatile halogenated solvents using a cleft-shaped 4-amino-1,8-naphthalimide Tröger's base fluorophore†‡

Binduja Mohan, Deivasigamani Umadevi and Sankarasekaran Shanmugaraju *

**A cleft-shaped 2-picolyl-4-amino-1,8-naphthalimide Tröger's base (TBNap) was synthesized and employed as a fluorescent 'turn-on' chemosensor for the discriminative sensing of volatile halogenated solvents based on an ICT sensing mechanism. TBNap displayed comparatively high fluorescence emission enhancement for chloroform – a potent anesthetic agent and a major constituent of tobacco smoke. The discriminative fluorescence sensing was also seen through visual color changes and was further validated using computational calculations.**

## Introduction

The design of easily adaptable sensing methods for detecting volatile organic solvents (VOSs) has attracted widespread research attention recently because of their serious menace to the living system and severe environmental pollution.[1–5] Volatile halogenated solvents (VHSs) are one type of VOSs with one or more halogen atoms.[6,7] The widespread usage of VHSs in numerous industrial settings and research laboratories increases the risk of serious environmental contamination and workplace explosions owing to their high volatility.[8,9] Several health hazards due to excessive exposure to the vapors of VHSs include eye irritation, heart diseases, intensive headaches, kidney failure, and respiratory malfunction, all of which could be fatal, and halogenated solvents are also known to cause cancer.[10–13]

In general, VHSs are harmful and difficult to decompose; thus, VHSs must be treated or transformed into innocuous products before releasing to the atmosphere.[14,15] VHSs can also react in the atmosphere to produce several toxic gaseous species.[16] Consequently, the precise detection and differentiation of VHSs are of significant importance and are acknowledged as a prerequisite for their appropriate use and effective treatment. Therefore, developing a suitable sensing method for the discriminative sensing of VHSs is important to mitigate their detrimental effect on human health and the environment. Several analytical techniques, including high-performance chromatography, FT-IR spectroscopy, and gas-chromatography mass-spectrometry (GC-MS), are available to detect VHSs.[17–19] However, the tedious and multi-step procedure, high-maintenance cost, requirement of a trained operator, and inoperable on-field analysis restrict the applications of these instrumental techniques for the efficient detection and monitoring of VHSs. Hence, there is an increased interest in developing simple and cost-effective sensor systems for precisely sensing VHSs.

Because of its various advantageous features, such as simple operation, cost-effective instrumentation, unique selectivity, high sensitivity, fast-sensing responses, and easy visualization, fluorescence-based sensing has evolved as an effective detection method.[20–25] Many solvatochromic fluorescence probes have been reported for the discriminative sensing of VOSs.[26–28] The fluorescence emission of solvatochromic probes highly depends on the solvent polarity, and slight changes in the polarity of the medium can greatly affect their fluorescence emission properties. Until now, a wide variety of solvatochromic fluorescence sensors have been known. Most of them are limited in their practical applications due to their low fluorescence quantum yield, less molar absorption coefficient, and poor photostability.[29,30]

4-amino-1,8-naphthalimide Tröger's bases (**TBNaps**) belong to a significant class of 'V-shaped' supramolecular scaffolds with tremendous applications in chemosensing, medicinal and materials chemistry.[31–34] Owing to their unique cleft structure with a large-hydrophobic cavity and strong fluorescence emission due to internal-charge transfer (ICT) transition, **TBNaps** have been used as potential hosts in selective complexation of suitable guests and as fluorescence

*Department of Chemistry, Indian Institute of Technology Palakkad, Palakkad-678557, Kerala, India. E-mail: shanmugam@iitpkd.ac.in*

† We dedicate this article to Prof. Thorfinnur Gunnlaugsson on the occasion of his 55th birthday.

‡ Electronic supplementary information (ESI) available: FTIR, $^{13}C$ NMR, and HRMS of **TBNap**. Electronic absorption and fluorescence emission spectral data of **TBNap** are available. See DOI: https://doi.org/10.1039/d2sd00177b

chemosensors for the detection of numerous analytes.[1,28,31–34] Herein, we report a new 'turn-on' fluorescence sensor, bis-[*N*-(2-pyridyl)methyl)]-9,18-methano-1,8-naphthalimide-[*b*,*f*][1,5]diazocine (**TBNap**, see Scheme 1), for the discriminative fluorescence sensing of closely-related VHSs. **TBNap** exhibited a relatively high fluorescence enhancement for $CHCl_3$ over other structurally similar VHSs. **TBNap** can also be used as a naked-eye fluorescence sensor for discriminative identification of VHSs in the solution phase.

# Experimental

### Materials and methods

All reagents, solvents, and starting materials were purchased from Sigma-Aldrich and were used as received. Commercially available reagent-grade chemicals were used for the synthesis of **Nap** and **TBNap**. High-purity analytical grade halogenated solvents were purchased from Merck and used as received. Commercially available spectroscopy-grade solvents from Merck were used without further purification. 4-Nitro-1,8-naphthalic anhydride, 2-picolylamine, Pd/C (10%), hydrazine monohydrate ($H_2N–NH_2·H_2O$), paraformaldehyde, and trifluoroacetic acid (TFA) were purchased from Sigma-Aldrich were reagent grade and used as received. A deuterated solvent, $(CD_3)_2SO$, used for NMR analyses was purchased from Sigma-Aldrich. The precursors, *N*-[(2-pyridyl)methyl]-4-nitro-1,8-naphthalimide and *N*-[(2-pyridyl)methyl]-4-amino-1,8-naphthalimide (**Nap**), were synthesized following the procedure reported in the literature.[32,35]

An electrochemical IA9000 digital melting point apparatus was used for measuring the melting point of **TBNap** in an unsealed capillary tube. The Shimadzu Scientific Instruments (IR Tracer 100) equipped with an ATR sampler were used for recording the FT-IR spectrum. All NMR spectra were recorded on a Bruker-DPX-Avance spectrometer operating at 400 MHz for $^1$H NMR and 101 MHz for $^{13}$C NMR in a commercially available deuterated solvent. Chemical shifts are reported in parts-per-million (ppm) relative to the internal solvent $(CD_3)_2SO$. All NMR data were processed with Bruker Win-NMR 5.0, Topspin, and MestReNova software. Multiplicities were abbreviated as follows: singlet (s), doublet (d), and triplet (t). HRMS was performed on a Shimadzu mass spectrometer using positive ionization and a linear detector. The *m*/*z* values were recorded over a range of 100–2000. HPLC-grade $CH_3CN$ or $CH_3OH$ were used as carrier solvents. The UV-visible absorption spectra were recorded in a 1 cm quartz cuvette on a Thermo Fisher scientific spectrometer, and baseline correction was applied for all spectra. The emission spectra for all the experiments were recorded on a Perkin Elmer FL-8500 fluorescence spectrophotometer equipped with a xenon arc (150 W) light source. The temperature was kept constant throughout the measurements at 298 K. All spectroscopic measurements were recorded in a quartz cuvette with a scan rate of 1200 nm min$^{-1}$. The pH-dependent emission studies were performed using an OAKLON pH 550 meter. The obtained results were plotted using Origin Pro 8.5 software.

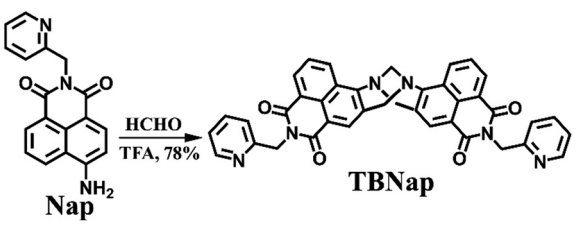


Scheme 1 Synthesis of **TBNap** from **Nap**.

### Synthesis of bis-[*N*-(2-pyridyl)methyl)]-9,18-methano-1,8-naphthalimide-[*b*,*f*][1,5]diazocine (TBNap)

Compound **Nap** (100 mg, 0.33 mmol, 1 equiv.) and paraformaldehyde (15 mg, 0.49 mmol, 1.5 equiv.) were taken in a 25 mL RB flask and flushed with nitrogen. Trifluoroacetic acid (3 mL) was added at 0 °C, and the solution was stirred at room temperature for 12 h under a nitrogen atmosphere. The reaction mixture was then added dropwise to aqueous ammonium hydroxide (30 mL) at 0 °C, and ammonia solution was added until a pH > 10 was achieved. The residue was extracted in dichloromethane (2 × 100 mL), and the organic layer was washed successively with saturated $NaHCO_3$ (2 × 30 mL), brine (2 × 30 mL) and $H_2O$ (2 × 30 mL). The solution was dried over $MgSO_4$, and the solvents were removed under reduced pressure to isolate compound **TBNap** (167 mg, 0.26 mmol, 78%) as a bright-yellow powder after trituration with cold-diethyl ether. Melting point 280–283 °C (decomp.). HRMS *m*/*z*: calcd for $C_{39}H_{27}N_6O_4$ [M + H$^+$] 643.21, found 643.25; $^1$H NMR (400 MHz, DMSO-$d_6$) $\delta$ 8.77–8.75 (2H, d, $J$ = 8.0 Hz, Naph-H), 8.48–8.46 (2H, d, $J$ = 8.0 Hz, Naph-H), 8.31–8.30 (2H, d, $J$ = 4.0 Hz, picolyl-H), 8.12 (2H, s, Naph-H), 7.99–7.97 (2H, t, $J$ = 8.0 Hz, Naph-H), 7.69–7.65 (2H, t, $J$ = 16 Hz, picolyl-H), 7.28–7.26 (2H, d, $J$ = 8 Hz, picolyl-H), 7.19–7.17 (2H, t, $J$ = 8 Hz, picolyl-H), 5.29 (4H, s, $CH_2$–H), 5.20–5.16 (2H, $J$ = 16 Hz, $NCH_2$–H), 4.74–4.70 (1H (s), 2H (d), $J$ = 16 Hz, $NCH_2$–H); $^{13}$C NMR (101 MHz, DMSO-$d_6$) $\delta$ 163.93, 163.35, 156.28, 149.75, 149.30, 137.11, 131.42, 131.00, 130.90, 129.86, 128.09, 127.72, 127.32, 126.75, 122.81, 122.51, 121.20, 118.02, 67.59, 57.25, 44.51; FT-IR $\nu_{max}$ (ATR, cm$^{-1}$) 3554, 3068, 2953, 1697, 1654, 1618, 1591, 1570, 1510, 1475, 1460, 1435, 1404, 1377, 1332, 1294, 1259, 1234, 1168, 1153, 1130, 1089, 1051, 1028, 1012, 962, 945, 914, 869, 837, 804, 785, 754, 686, 661, 630, 609, 574, 555, 518, 476.

### Fluorescence sensing studies

The stock solution (0.15 mM) of **TBNap** in the selected volatile halogenated solvents was prepared and utilized for spectroscopic titration studies. The emission spectra were recorded by diluting 200 μL stock solution of **TBNap** in the respective VHS with 1800 μL of the corresponding VHS in a quartz cell of 1 cm width. A similar titration procedure was carried out for all the VHSs separately, and changes in the emission pattern were measured. For the titration

experiment, 100 μL of **TBNap** stock solution in $CCl_4$ was diluted to 1000 μL using fresh $CCl_4$, and emission changes were recorded. Chloroform was incrementally added to the above solution (10 μL each), and the spectra were recorded at an excitation wavelength ($\lambda_{ex}$) of 380 nm, an excitation slit width of 10 nm, and an emission slit width of 5 nm.

### pH-dependent emission studies

To the 0.01 mM solution of **TBNap**, 1.0 mM HCl solution was added gradually to prepare acidic solutions, and the pH of the solution was determined, followed by the recording of fluorescence emission spectra at different pHs. The basic solution was prepared by adding 1.0 mM NaOH solution to the 0.01 mM solution of **TBNap**, and the fluorescence emission was measured at different pHs of the solution. All the measurements were performed at room temperature.

## Results and discussion

### Synthesis and characterization of TBNap

As shown in Scheme 1, the chemosensor **TBNap** was synthesized from its corresponding amine precursor, *N*-(2-pyridyl)methyl-4-amino-1,8-naphthalimide (**Nap**), which was readily obtained from *N*-(2-pyridyl)methyl-4-nitro-1,8-naphthalimide *via* Pd/C mediated catalytic hydrogenation reaction.[33,35] The cyclization of freshly synthesized **Nap** with paraformaldehyde (1.5 equiv.) in trifluoroacetic acid yielded the desired product **TBNap** as a bright-yellow powder in a 78% isolated yield (for details, see the Experimental section). **TBNap** was soluble in most common solvents and was fully analyzed using various standard spectroscopic techniques, such as FT-IR, multinuclear ($^1$H and $^{13}$C) NMR, and HRMS. Further, the structure of **TBNap** was modeled using computational calculations.

The FT-IR spectrum of **TBNap** displays the characteristic $C{=}O_{imide}$, $C{=}N_{pyridyl}$, and $C{-}N_{Tröger's\ base}$ functional group stretching vibrational bands at $\nu$ = 1697, 1652 and 1232 $cm^{-1}$, respectively (Fig. S1, ESI‡). In the $^1$H NMR spectrum of **TBNap** recorded in DMSO-$d_6$, the presence of two-well resolved doublets in the range of $\delta$ = 5.20–4.69 ppm corresponds to the methylene (–$CH_2$N–) proton resonances of the bridge-head diazocine unit. The aromatic proton signals for the 2-picolyl and 1,8-naphthalimide moieties were observed between $\delta$ = 8.77 and 7.17 ppm. The 2-picolyl methylene ($CH_2$) proton resonance appeared at $\delta$ = 5.29 ppm (Fig. 1A). The high-resolution mass-spectrometry (HRMS) analysis showed an intense peak at $m/z$ = 643.2074 corresponding to the $[M + H]^+$ molecular ion (Fig. S3, ESI‡). The energy-minimized structure of **TBNap** demonstrates its unique cleft-shaped conformation, in which the bridge-head diazocine unit with an angle of 95.86° places the two 1,8-naphthalimide moieties perpendicular to each other at an inter-planar distance of 7.29 Å. Notably, the two 2-picolyl moieties are flanked outwards from the hydrophobic cavity, possibly to avoid the steric hindrance (Fig. 1B). **TBNap** is a typical push–pull type of fluorophore, which is evidenced by

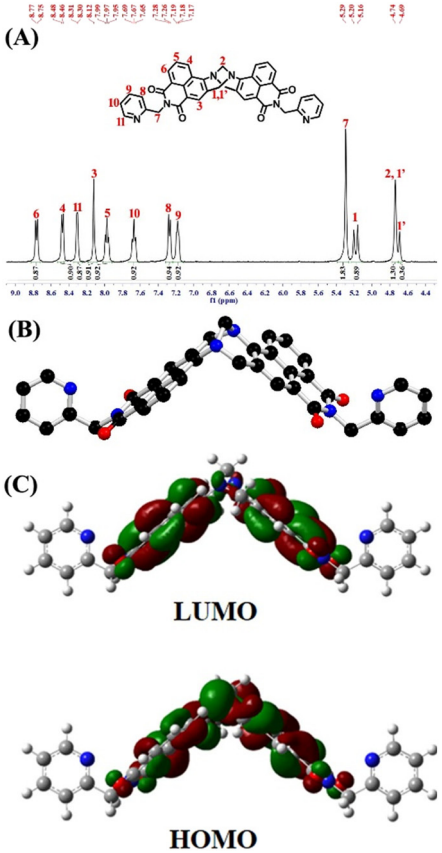


**Fig. 1** (A) $^1$H NMR spectrum of **TBNap** (400 MHz, DMSO-$d_6$) with peak assignment. (B) Energy-minimized structure of **TBNap** (colour code: black C, red O, and blue N). Hydrogen atoms are omitted for clarity. (C) The frontier molecular orbitals of **TBNap**.

the electron-density distribution. The HOMO electron density is more localized on the Tröger's base moiety. At the same time, the LUMO is primarily distributed at the imide unit (Fig. 1C). Therefore, on excitation, there is an internal-charge transfer transition from the electron-rich Tröger's base moiety to the electron-deficient imide sites, which makes **TBNap** a highly emissive fluorophore.

### Fluorescence sensing studies

After the successful synthesis and characterization, we next analyzed the photophysical properties of **TBNap** in various organic solvents. **TBNap** was dissolved/well-dispersed in different solvents, namely, chloroacetyl chloride (CAC), tetrachloromethane (TCM), chloroform (CFM), cyclohexyl bromide (CHB), dichloromethane (DCM), dichloroethane (DCE) and epichlorohydrin (ECH), bromobenzene (BrB), butyl-benzene (BuB), propyl-benzene (PrB), tetrahydrofuran (THF) and acetonitrile (ACN). The UV-vis absorption spectra of **TBNap** in different organic solvents display the characteristic bands of a high-energy absorption band at $\lambda$ = 340–355 nm corresponding to the π–π* transition and a low-energy broad band centered at $\lambda$ = 348–385 nm ascribed to the internal charge transfer (ICT) transition (Fig. S4, ESI‡). It

is worth mentioning that no significant shift in the absorption maxima ($\lambda_{max}$) was observed in the electronic absorption spectra of **TBNap** recorded in different organic solvents (except in chloroacetyl chloride), and this indicates that the solvent effect in the ground state was inconsequential. However, the notable differences in the absorption intensity in different solvents were presumably due to their solubility difference in the selected solvents (Fig. S4, ESI‡).

The fluorescence emission spectra of **TBNap** were measured in various organic solvents. As expected, **TBNap** in different solvent media exhibited various fluorescence emission profiles. The calculated quantum yield for **TBNap** in different solvents was in the range of $\phi$ = 0.05 to 4.15 (see Table S1, ESI‡). The pH-dependent fluorescence emission studies revealed that at basic pH > 8, **TBNap** was highly emissive, but at acidic pH < 4, the emission intensity decreased due to the protonation of the $NH_2$ group (Fig. S5, ESI‡). Furthermore, the concentration-dependent fluorescence emission study showed that the emission intensity of **TBNap** was enhanced upon gradually increasing its concentration (Fig. S6, ESI‡). Among various organic solvents, interestingly, **TBNap** in chloroform (CFM) medium displayed the highest fluorescence emission intensity, which is accompanied by significant redshifts in emission maxima ($\lambda_{max}$) (Fig. 2A and B). From the emission profile, the relative number-fold emission enhancement was calculated by taking **TBNap** in tetrachloromethane (TCM) as the reference medium. Among the chosen solvents, **TBNap** in CFM solution displayed the highest number-fold emission change of about 9.3. In contrast, the CAC solution displayed the least value of 0.3 (Fig. 2C). The fluorescence emission enhancement order was as follows: CFM > BrB > PrB > DCM > BuB > CHB > DCE > THF > ECH > ACN > CAC. These variations in the emission intensity pattern in different solvents demonstrate that **TBNap** can clearly distinguish the closely related VHSs and sense a particular solvent system. Notably, the observed difference in fluorescence enhancement among the chosen chlorinated solvents indicates that no photodissociation occurs in the solution, and the discriminative fluorescence sensing of VHSs is primarily due to the difference in the solvent polarity.

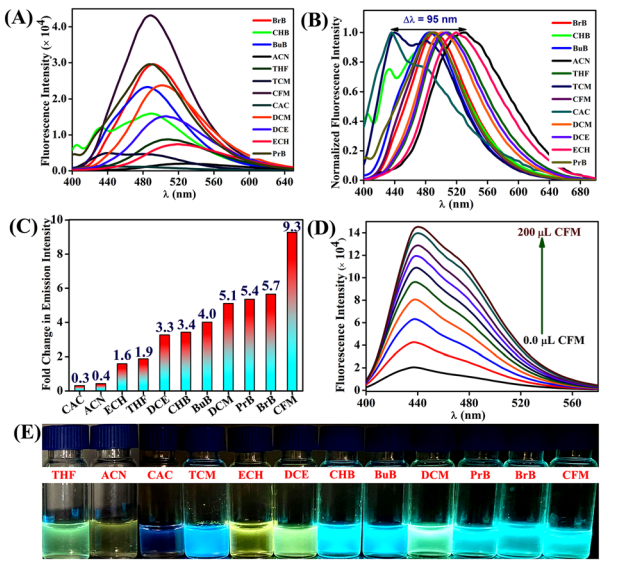


**Fig. 2** (A) The measured relative changes in the fluorescence emission intensity of **TBNap** in different organic solvents and (B) the corresponding normalized emission spectra showing the bathochromic shift in the emission maxima. (C) Number-fold changes in the emission intensity of **TBNap** concerning its emission in TCM. (D) The observed increases in the fluorescence emission of **TBNap** dissolved in $CCl_4$ upon increasing the volume percentage of CFM. (E) The photograph of the visual color change was imaged in different organic solvents under UV-light irradiation.

To get further insight into the fluorescence sensing properties of **TBNap**, we performed fluorescence titration studies in a CFM medium. Upon incremental volume addition of CFM to **TBNap** solution in TCM, we observed a gradual increase in the fluorescence emission intensity at $\lambda_{max}$ = 440 nm (Fig. 2D). From the titration profile, the plot between the fluorescence emission enhancements and the volume percentage of CFM displays a linear relationship with a slope of $1.8 \times 10^4$. This linear curve indicates the potential of **TBNap** to quantitatively determine the volume percentage of the CFM content in other organic solvent media (Fig. S7, ESI‡). In addition, the normalized fluorescence emission spectra of **TBNap** in the chosen solvents display a perfect bathochromic shift ($\Delta\lambda$ = 95 nm) from the blue to the red region (Fig. 2B). Solvents with a high dielectric constant exhibited emission at a higher wavelength, and solvents with a low dielectric constant emitted in the low-wavelength region. For example, **TBNap** in TCM with a dielectric constant of 2.24 exhibited the emission maxima at $\lambda$ = 436 nm. In contrast, **TBNap** in ACN, having a ten times higher dielectric constant (37.5), displayed the emission maxima at $\lambda$ = 530 nm (see Table S1, ESI‡). The redshift was due to the stabilization of the excited-state dipole of **TBNap** in the solvent medium with a high dielectric constant that decreases the HOMO–LUMO energy difference and enhances the possibility of strong ICT transition leading to an increase in the wavelength.[7] On top of this, **TBNap** can effectively discriminate the chosen closely-related VHSs *via* naked-eye visualization (Fig. 2E). The shift in color of **TBNap** from blue to yellow as a function of an increase in the solvent dielectric constant was observed under a UV lamp. In particular, the commonly used volatile halogenated solvents TCE, CFM, and DCM, with a slight difference in their structure, displayed a remarkable shift in the color from blue to green, respectively, which is even observable with the naked eye (Fig. S8, ESI‡). Thus, the developed sensor **TBNap** can be used as a practically useful colorimetric probe for discriminative sensing of volatile halogenated solvents.

The observed discriminative 'turn-on' fluorescence sensing of **TBNap** in different VHSs was further validated by computational analysis using density functional theory (DFT) calculations. All the calculations were done at the B3LYP/6-311++G**//B3LYP/6-31G* level of theory by using the

Table 1 The HOMO and LUMO energies of **TBNap** and various VHSs compared to the number-fold emission enhancement

| Compounds | HOMO (eV) | LUMO (eV) | Fold-changes in emission intensity |
|---|---|---|---|
| **TBNap** | −6.298 | −2.694 | — |
| CFM | −8.752 | −1.595 | 9.3 |
| BrB | −6.906 | −0.887 | 5.7 |
| PrB | −7.574 | −0.701 | 5.4 |
| DCM | −8.594 | −0.913 | 5.1 |
| BuB | −7.557 | −0.621 | 4.0 |
| CHB | −7.442 | −0.653 | 3.4 |
| DCE | −8.322 | −0.607 | 3.3 |
| ECH | −7.972 | −0.483 | 1.6 |

Gaussian 16 program.[36] We calculated the HOMO and LUMO energies of all the chosen VHSs and compared them with **TBNap** frontier molecular orbitals. As given in Table 1, the calculated LUMO energy of all the chosen solvents was found to be higher in energy than the LUMO energy of **TBNap**, which favors the possibility of energy transfer from VHSs to **TBNap** and, thus, results in the fluorescence emission enhancement. The calculated energy difference between the LUMO of CFM and **TBNap** was comparatively low, which indicates the enhanced energy transfer from CFM to **TBNap** and, therefore, a greater fluorescence enhancement. The order of emission enhancement is in good agreement with the calculated energy differences and dielectric constants of various VHSs, which supports that the observed discriminative fluorescence 'turn-on' sensing of VHSs follows an ICT-based sensing mechanism.

## Conclusions

In conclusion, we have carefully designed and developed a novel 2-picolyl-4-amino-1,8-naphthalimide Tröger's base (**TBNap**) and demonstrated its application as a turn-on fluorescence sensor for the discriminative sensing of volatile halogenated solvents. The "N" containing picolyl and Tröger's base moieties improve the utilization of **TBNap** for halogenated solvent sensing. The sensor **TBNap** showed a higher fluorescence enhancement in the CFM solvent compared to the other solvent medium. The enhancement behavior was validated using computational analysis. In addition to sensing, **TBNap** has also been used for the trace quantification of volatile solvents. The discriminative fluorescence sensing was also evident from the visual color changes, thereby upgrading the practical applicability of **TBNap** as a colorimetric probe. Further studies are in progress to develop a practically useful **TBNap**-based sensor system with improved selectivity, specificity, and sensitivity for detecting particular volatile solvents.

## Author contributions

Binduja Mohan: data curation, formal analysis, investigation, methodology, software, validation, and writing – original draft. Deivasigamani Umadevi: computational investigation and validation. Sankarasekaran Shanmugaraju: conceptualization, funding acquisition, project administration, resources, supervision, validation, visualization, and writing – original draft.

## Conflicts of interest

There are no conflicts to declare.

## Acknowledgements

The authors thank the Science and Engineering Research Board (EMEQ Award EEQ/2018/000799 to SS) for the financial support. We thank the Central Instrumentation Facility (CIF) at IIT Palakkad for the research facilities.

## References

1 S. Shanmugaraju, D. Umadevi, L. M. González-Barcia, J. M. Delente, K. Byrne, W. Schmitt, G. W. Watson and T. Gunnlaugsson, *Chem. Commun.*, 2019, **55**, 12140.
2 H. Liu, X. Xu, Z. Shi, K. Liu and Y. Fang, *Anal. Chem.*, 2016, **88**, 10167.
3 L. Vittozzi and E. Testai, *Handbook of Hazardous Materials*, Academic Press, 1993, pp. 119–125.
4 R. F. Landis, M. Yazdani, B. Creran, X. Yu, V. Nandwana, G. Cooke and V. M. Rotello, *Chem. Commun.*, 2014, **50**, 4579.
5 A. Bergen, C. Bohne, D. Fuentealba, H. Ihmels, T. Pace, M. Waidelich, C. Yihwa and J. W. Bats, *Photochem. Photobiol. Sci.*, 2012, **11**, 752.
6 C. Bohne, H. Ihmels, M. Waidelich and C. Yihwa, *J. Am. Chem. Soc.*, 2005, **127**, 17158.
7 L. Dai, D. Wu, Q. Qiao, W. Yin, J. Yin and Z. Xu, *Chem. Commun.*, 2016, **52**, 2095.
8 R. Parui, N. Meher and P. K. Iyer, *Mater. Adv.*, 2022, **3**, 5980.
9 R. Gao and D. Yan, *Chem. Commun.*, 2017, **53**, 5408.
10 J. K. Wickliffe, T. H. Stock, J. L. Howard, E. Frahm, B. R. SimonFriedt, K. Montgomery, M. J. Wilson, M. Y. Lichtveld and E. Harville, *Sci. Rep.*, 2020, **10**, 21649.
11 B. Huang, C. Lei, C. Wei and G. Zeng, *Environ. Int.*, 2014, **71**, 118.
12 C. Barragán-Martínez, C. A. Speck-Hernández, G. Montoya-Ortiz, R. D. Mantilla, J.-M. Anaya and A. Rojas-Villarraga, *PLoS One*, 2012, **7**, e51506.
13 N. Guha, D. Loomis, Y. Grosse, B. Lauby-Secretan, F. E. Ghissassi, V. Bouvard, L. Benbrahim-Tallaa, R. Baan, H. Mattock and K. Straif, *Lancet Oncol.*, 2012, **13**, 1192.
14 W. I. S. Galpothdeniya, B. P. Regmi, K. S. McCarter, S. L. de Rooy, N. Siraj and I. M. Warner, *Anal. Chem.*, 2015, **87**, 4464.
15 J. Lee, H. T. Chang, H. An, S. Ahn, J. Shim and J.-M. Kim, *Nat. Commun.*, 2013, **4**, 2461.
16 W. R. Simpson, S. S. Brown, A. Saiz-Lopez, J. A. Thornton and R. V. Glasow, *Chem. Rev.*, 2015, **115**, 4035.
17 W. Buchberger and U. Huebauer, *Microchim. Acta*, 1989, **99**, 137.

18 M. I. Cervera, J. Beltran, F. J. Lopez and F. Hernandez, *Anal. Chim. Acta*, 2011, **704**, 87.
19 R. Lu, W.-W. Li, B. Mizaikoff, A. Katzir, Y. Raichlin, G.-P. Sheng and H.-Q. Yu, *Nat. Protoc.*, 2016, **11**, 377.
20 X. Zhou, S. Lee, Z. Xu and J. Yoon, *Chem. Rev.*, 2015, **115**, 7944.
21 A. P. de Silva, H. Q. N. Gunaratne, T. Gunnlaugsson, A. J. M. Huxley, C. P. McCoy, J. T. Rademacher and T. E. Rice, *Chem. Rev.*, 1997, **97**, 1515.
22 S. Erbas-Cakmak, S. Kolemen, A. C. Sedgwick, T. Gunnlaugsson, T. D. James, J. Yoon and E. U. Akkaya, *Chem. Soc. Rev.*, 2018, **47**, 2228.
23 G. Sivaraman, B. Vidya and D. Chellappa, *RSC Adv.*, 2014, **4**, 30828.
24 T. Shen, D. Tan, M. Shanmugham and X. Liu, *Sens. Diagn.*, 2022, **1**, 714.
25 S. Shanmugaraju and P. S. Mukherjee, *Chem. Commun.*, 2015, **51**, 16014.
26 E. Yamaguchi, C. Wang, A. Fukazawa, M. Taki, Y. Sato, T. Sasaki, M. Ueda, N. Sasaki, T. Higashiyama and S. Yamaguchi, *Angew. Chem., Int. Ed.*, 2015, **127**, 4622.
27 L. Giordano, V. V. Shvadchak, J. A. Fauerbach, E. A. Jares-Erijman and T. M. Jovin, *J. Phys. Chem. Lett.*, 2012, **3**, 1011.
28 S. Shanmugaraju, C. Dabadie, K. Byrne, A. J. Savyasachi, D. Umadevi, W. Schmitt, J. A. Kitchen and T. Gunnlaugsson, *Chem. Sci.*, 2017, **8**, 1535.
29 R. F. Landis, M. Yazdani, B. Creran, X. Yu, V. Nandwana, G. Cooke and V. M. Rotello, *Chem. Commun.*, 2014, **50**, 4579.
30 J. Yoon, Y. Jung and J. Kim, *Adv. Funct. Mater.*, 2009, **19**, 209.
31 E. B. Veale and T. Gunnlaugsson, *J. Org. Chem.*, 2010, **75**, 5513.
32 S. Shanmugaraju, C. S. Hawes, A. J. Savyasachi, S. Blasco, J. A. Kitchen and T. Gunnlaugsson, *Chem. Commun.*, 2017, **53**, 12512.
33 M. Binduja, E.-A. Sandra, D. Umadevi, B. C. Poulsen, S. Blasco, G. J. McManus, T. Gunnlaugsson and S. Shanmugaraju, *Inorg. Chem.*, 2022, **61**, 11592.
34 J. M. Delente, D. Umadevi, S. Shanmugaraju, O. Kotova, G. W. Watson and T. Gunnlaugsson, *Chem. Commun.*, 2020, **56**, 2562.
35 J. I. Lovitt, D. Umadevi, P. Raja Lakshmi, B. Twamley, T. Gunnlaugsson and S. Shanmugaraju, *Supramol. Chem.*, 2020, **32**, 620–633.
36 M. J. Frisch, G. W. Trucks, H. B. Schlegel, G. E. Scuseria, M. A. Robb, J. R. Cheeseman, G. Scalmani, V. Barone, G. A. Petersson, H. Nakatsuji, X. Li, M. Caricato, A. V. Marenich, J. Bloino, B. G. Janesko, R. Gomperts, B. Mennucci, H. P. Hratchian, J. V. Ortiz, A. F. Izmaylov, J. L. Sonnenberg, D. Williams-Young, F. Ding, F. Lipparini, F. Egidi, J. Goings, B. Peng, A. Petrone, T. Henderson, D. Ranasinghe, V. G. Zakrzewski, J. Gao, N. Rega, G. Zheng, W. Liang, M. Hada, M. Ehara, K. Toyota, R. Fukuda, J. Hasegawa, M. Ishida, T. Nakajima, Y. Honda, O. Kitao, H. Nakai, T. Vreven, K. Throssell, J. A. Montgomery, Jr., J. E. Peralta, F. Ogliaro, M. J. Bearpark, J. J. Heyd, E. N. Brothers, K. N. Kudin, V. N. Staroverov, T. A. Keith, R. Kobayashi, J. Normand, K. Raghavachari, A. P. Rendell, J. C. Burant, S. S. Iyengar, J. Tomasi, M. Cossi, J. M. Millam, M. Klene, C. Adamo, R. Cammi, J. W. Ochterski, R. L. Martin, K. Morokuma, O. Farkas, J. B. Foresman and D. J. Fox, *Gaussian 16, Revision C.01*, Gaussian, Inc., Wallingford CT, 2016.